JOURNAL OF MATERIALS SCIENCE 33 (1998) 1083–1089

Analysis of the spatial distribution of Y_2BaCuO_5 inclusions in large-grain $YBa_2Cu_3O_{7-\delta}$

J. C. L. CHOW, H.-T. LEUNG, WAI LO, D. A. CARDWELL
IRC in Superconductivity, University of Cambridge, Madingley Road, Cambridge, CB3 0HE, UK

High values of critical current density, J_c, in large-grain superconducting melt-processed $YBa_2Cu_3O_{7-\delta}$ (YBCO, Y-123) have been reported to correlate closely with the distribution of Y_2BaCuO_5 (Y-211) particles in the Y-123 phase matrix. Extensive image analysis of the homogeneity of the Y-211 particle distribution in a large-grain sample has been performed on high-resolution, secondary scanning electron micrographs of seeded melt-processed YBCO. The variation of key parameters, such as area fraction, number density and size along the *a*/*b* axis of the Y-123 grain has been investigated in detail as a function of distance from the centre of the seed. Both area fraction and number density of Y-211 particles are observed to increase continuously with distance, whereas the mean and standard deviation of the size distribution decrease slightly towards the grain boundary. This suggests that the increase in area fraction can be attributed to an increase in number density of the Y-211 particle distribution along the *a*/*b* axis of the specimen. The implications for Y-211 particle pushing, ripening and coalescence are discussed in the light of these results.

1. Introduction

High-temperature superconducting (HTS) $YBa_2Cu_3O_{7-\delta}$ (YBCO) has significant potential for a variety of engineering applications such as magnetic bearings, fault current limiters and flywheel energy storage systems [1–5]. The flux trapping ability of bulk YBCO, which generally forms the basis of these applications, depends fundamentally on the magnitude and homogeneity of the critical current density, J_c, of the material and the length scale over which it flows [6]. In particular, the presence of grain boundaries and intragrain domains can limit J_c significantly and these are clearly undesirable features of bulk material. A main processing aim, therefore, is to develop a large-grain material with a high J_c which flows over the entire grain geometry. This has been achieved by a variety of peritectic solidification, or melt process, techniques that have been developed over recent years to fabricate large-grain YBCO. These have yielded J_cs of up to 10^5 A cm^{-2} at 77 K in grains of typically 1 cm in diameter [7–13].

A characteristic feature of melt-processed YBCO is the presence of non-superconducting Y_2BaCuO_5 (Y-211) phase inclusions in the superconducting $YBa_2Cu_3O_{7-\delta}$ (Y-123) phase matrix [2, 14–16]. The distribution, size, number density and shape of Y-211 particles have been observed to correlate closely with J_c [17–19] and, as such, are key parameters in the development of a practical material. Of these, a homogeneous Y-211 inclusion distribution in the Y-123 phase matrix has been identified as being particularly important in achieving uniform, high J_c in large-grain material.

The distribution of Y-211 particles in melt-processed YBCO is sensitive to both the crystallographic orientation of the grain and the rate of grain growth during fabrication. As a result, the Y-211 distribution in YBCO samples fabricated by most melt-processed techniques is invariably inhomogeneous, particularly when observed along the *a*/*b* crystallographic directions of the grain [20]. Several mechanisms have been employed to explain this inhomogeneity including particle pushing theory [20, 21], which is commonly applied to other, unrelated material systems such as metal matrix composites (MMC) [22, 23], ripening theory [24] and coalescence [25] theory. A detailed experimental analysis of the spatial distribution of the Y-211 particles in the Y-123 matrix of melt-processed YBCO is required to understand the origin of any inhomogeneity in view of this range of potential mechanisms. Information gleaned from such a study could also be significant from a processing point of view since it could contribute to the fabrication of bulk material with improved superconducting properties.

Image analysis of sample microstructure is potentially a powerful tool in the investigation of the Y-211 particle distribution in melt-processed grains. This technique can be employed to provide statistical data on a number of key variables associated with the Y-211 phase, including size, orientation, shape and number density. Most micrograph image analysis has been performed on a variety of doped melt-processed samples using relatively low-resolution optical microscopy [26–29]. It is well known, however, that melt-processed YBCO invariably contains sub-micron sized Y-211 inclusions (the number density of such particles is enhanced significantly by platinum doping [30–32]) which are too small to be resolved by this technique (the resolution of optical microscopy is

typically $\sim 1\,\mu m$). Such a fine distribution of Y-211 particles is of particular interest since the J_c of these samples is typically much higher than that of samples containing larger-sized inclusions. As a result, an alternative imaging technique, such as scanning electron microscopy (SEM), has to be employed in order to image reliably the Y-211 distribution in samples which exhibit high critical current densities.

The operating mode of the scanning electron microscope requires some consideration if the product micrographs are to yield the most reliable image analysis results. For example, the secondary electron SEM image characteristically exhibits enhanced resolution but inferior topological contrast compared with the back-scattered electron image, which, in turn, offers improved contrast but at a resolution similar to that of the optical microscope. Contrast between the Y-211 particles and Y-123 matrix in melt-processed YBCO in the higher resolution secondary electron image, therefore, is usually achieved by etching the surface of the SEM specimen prior to imaging. The degree of etching in such a process is critical to obtaining a good image of the sample because an insufficient degree would limit the contrast of the scanning electron micrographs, whereas over-etching would reduce the size of the Y-211 particles as well as create other artificial features of the secondary phases on the sample surface [33].

The aim of the present study was to perform a systemic and accurate image analysis of Y-211 inclusions in large-grain melt-processed YBCO.

2. Experimental procedure

2.1. Sample fabrication

Precursor powder was prepared by spray drying a nitrate solution of the base metal cations in a molar ratio of $Y:Ba:Cu = 1.6:2.3:3.3$, corresponding to a net composition of Y-123 + 30 mol % excess Y-211 (this composition reduces the loss of liquid from the sample during thermal processing [34, 35]). The advantages of the spray-drying technique for the preparation of fine, unreacted YBCO precursor powder is described elsewhere [36]. The powder was calcined for 35 h at 770 °C and uniaxially die pressed into pellets of diameter 2.5 cm. The pellets were sintered prior to melt processing to increase their density to $\sim 5.9\,g\,cm^{-3}$ [37].

A large-grain YBCO sample was fabricated via a seeded peritectic solidification technique described in detail elsewhere [38]. Briefly, the sintered precursor pellet was heated to 1025 °C (i.e. above the YBCO peritectic temperature of $\sim 1015\,^{\circ}C$ in air) at a rate of $10\,^{\circ}C\,h^{-1}$ and cooled at $120\,^{\circ}C\,h^{-1}$ to an isothermal solidification temperature of 985 °C. The pellet was then cooled slowly at $1\,^{\circ}C\,h^{-1}$ to 930 °C and more quickly to room temperature. Grain nucleation and growth was controlled by a single-crystal $SmBa_2Cu_3O_{6.5}$ (Sm-123) seed, which was placed at the centre of the upper surface of the precursor pellet prior to melt processing, and by thermal gradients of up to $15\,^{\circ}C\,cm^{-1}$ generated in a purpose-built box furnace with the aid of a cold finger [39]. The orientation of the seed, which determines the orientation of the melt-processed YBCO, was chosen such that its crystallographic *c*-axis was perpendicular to the surface of the pellet. This process yielded a large grain of rectangular geometry with dimensions $\sim 8 \times 8 \times 3\,mm^3$. The critical current density of the specimen was measured by a magnetic moment technique [40] to be $\sim 20\,000\,A\,cm^{-2}$ at 77 K in an applied magnetic field of 1 T.

2.2. SEM specimen preparation

The large YBCO grain was cut in half along the crystallographic *c*-axis (i.e. through its thickness to expose an *a*/*b*–*c* plane) using a diamond impregnated steel wire cutter in order to obtain a relatively smooth cross-section. The sample was then set in epoxy resin loaded with carbon powder and the exposed surface of the grain repeatedly ground and polished, ultimately with 0.25 μm diamond paste, to produce a smooth sample surface and to ensure that fine, sub-micron sized Y-211 particles could be identified in the *a*/*b*–*c* plane of the YBCO microstructure. Finally, the specimen was etched to improve the topological contrast between the Y-123 and Y-211 phases during microscopy by immersion in 3% HNO_3 acid for 3 s [35]. The sample was then washed immediately in distilled water to avoid over-etching, rinsed in methanol to remove any remaining water from the sample surface, and dried under a hot air jet at 80 °C. Care was taken throughout the specimen preparation process to avoid excessive polishing and etching which could damage the surface microstructure and hence introduce error into the subsequent image analysis.

2.3. Scanning electron microscopy and image analysis

A Cambridge Stereoscan S250 scanning electron microscope was used to investigate the microstructure and take micrographs of the YBCO specimen. A fine spot size and short working distance of 10 mm were employed in order to achieve the highest possible secondary electron image resolution of this instrument [41]. The contrast between the Y-123 and Y-211 phases was enhanced further by utilization of the gamma function available with the SEM [42]. These operating conditions yielded a high-magnification micrograph with a distinguishable Y-211 particle size down to $\sim 0.2\,\mu m$. Lower magnification micrographs of the YBCO microstructure were taken initially to confirm the orientation of the grain and to provide a position reference map for the higher magnification images. In total, over 60 high-magnification images were taken over individual areas of $\sim 50\,\mu m \times 40\,\mu m$ along the *a*/*b* axis of the grain at a constant position along the *c*-axis (i.e. across one *a*/*b*–*c* plane of the sample).

The high-resolution scanning electron micrographs were enlarged and copied onto transparencies in order to highlight the texture of Y-211 particles and pores in the YBCO grain microstructure. The

transparencies were then scanned and converted into standard graphic files using a high-resolution scanner for subsequent image analysis by Khoros software. Information on the Y-211 particle number density, size and area fraction was obtained from each micrograph by this rather labour-intensive technique.

3. Results and discussion

Fig. 1a shows a scanning electron micrograph taken near the centre of the specimen (i.e. in the vicinity of the Sm-123 seed) and illustrates the typical microstructure of Y-211 particles entrapped in the Y-123 matrix. Comparison of this micrograph with that in Fig. 1b, which was taken at the edge of the YBCO grain, illustrates a significant variation in the Y-211 particle area and number density as a function of distance from the seed in the *a–b* plane.

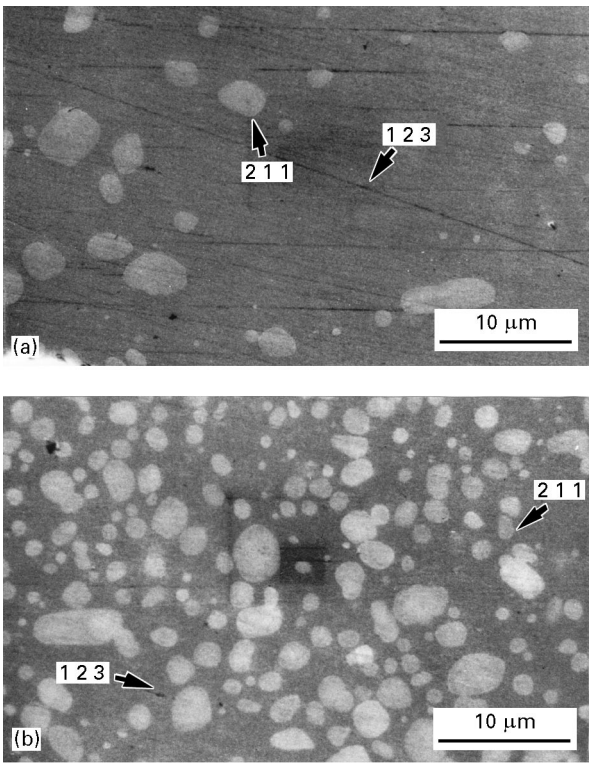

Figure 1 Scanning electron micrographs showing the inhomogeneous distribution of Y-211 particles (a) in the vicinity of the single crystal seed, and (b) at the edge of the large YBCO grain.

In general, the Y-211 particles can be characterized according to their position both in the scanning electron micrograph (i.e. intersecting the edge or corner) and relative to that of other particles (i.e. isolated, coalesced or touching). These combined features of the micrograph and Y-211 distribution significantly influence the results of image analysis. Hence it is necessary to subcategorise the Y-211 particles into six different statistical groups plus two further groups (pore and Y-123 matrix background), as defined in Table I. All eight groups are illustrated schematically in Fig. 2. A description of how the various sub-categories of Y-211 particles are assumed to contribute to the overall number density, area fraction and particle size is summarized in Table I.

The area fraction, F_{211}, and the number density, n_{211}, of Y-211 particles along the a/b direction of the grain were calculated using the counting criteria outlined above. The variation of these parameters with distance from the centre of the seed is plotted in Fig. 3a (F_{211}) and b (n_{211}). It is immediately apparent that both variables increase continuously with distance from the centre of the seed to the grain boundary. Furthermore, the close correlation between these parameters suggests that the increase in F_{211} may be attributed directly to the associated increase in n_{211}.

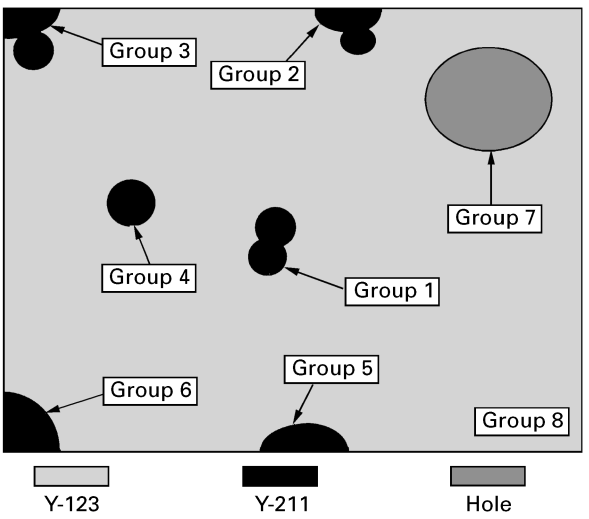

Figure 2 Schematic diagram illustrating the different categories of Y-211 particle in the scanning electron micrographs.

TABLE I Eight sub-categories of the Y-211 particle distribution and their contribution to the statistical analysis

Group number	Features	Contribution to number density, area fraction and particle size
1	Coalesced Y-211	Sub-categorized according to number of particles coalesced
2	Coalesced Y-211 intersecting the side of the micrograph	Counted as a half particle
3	Coalesced Y-211 intersecting the corner of the micrograph	Counted as a quarter particle
4	Single Y-211	Counted as one particle
5	Single Y-211 intersecting the side of the micrograph	Counted as a half particle
6	Single Y-211 intersecting the corner of the micrograph	Counted as a quarter particle
7	Pore	Subtracted from background in calculating area fraction
8	Background	Used to determine area fraction

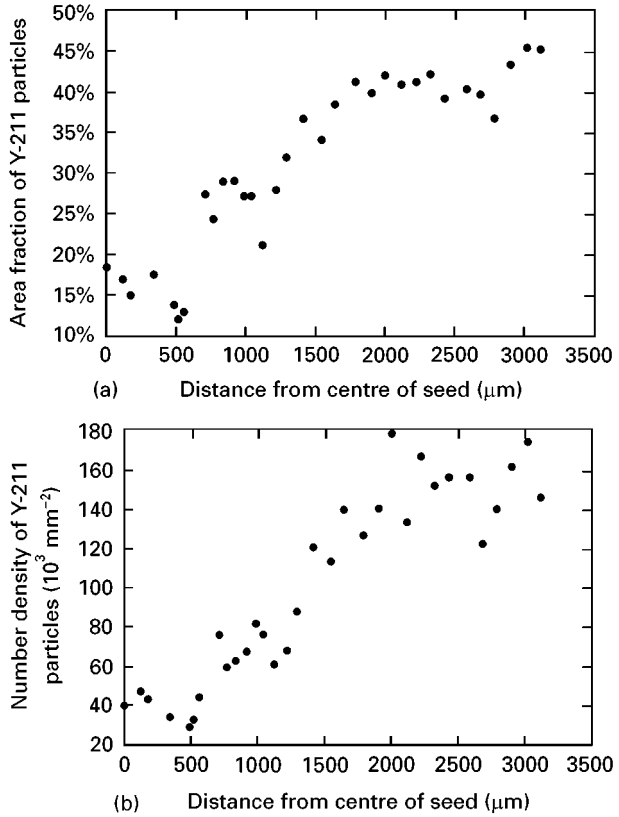

Figure 3 The variation of (a) area fraction, and (b) number density of Y-211 particles as a function of distance from the centre of the seed along the *a*/*b* direction of the grain.

Fig. 4 shows the size distribution of Y-211 particles at four different locations from the centre of the seed along the *a*/*b* direction of the grain (variation of the key Y-211 distribution parameters along the *c*-axis of the sample was not investigated in the present study). The Y-211 particle diameter, *d*, was calculated for the purposes of these plots via the following equation;

$$d = 2(\pi A)^{1/2} \quad (1)$$

where *A* is the area of the grain which is assumed to be of circular cross-sectional area. It is apparent from Fig. 4 that the Y-211 particle size distribution along the *a*/*b* direction of the grain follows a log-normal distribution [43] which does not vary within experimental error with distance from the single-crystal seed. A more detailed investigation of the characteristic log-normal distribution of Y-211 particles in the melt-processed YBCO matrix is the subject of an on-going study [44].

Fig. 5 shows the mean, μ, and standard deviation, σ, of Y-211 particles along the *a*/*b* direction, again as a function of distance from the seed. A decrease in μ is observed as the Y-123 grain develops, which is accompanied by a smaller reduction in standard deviation (Fig. 5a). Such a variation in these parameters cannot account for the increase in F_{211} shown in Fig. 3a, and provides further evidence for a direct correlation between F_{211} and n_{211}. It is also apparent from Fig. 5 that both μ and σ fluctuate significantly at a distance of approximately 1 mm from the centre of the seed. This is due to the rather low value of n_{211} at this position (Fig. 3b), which imposes a limit on the

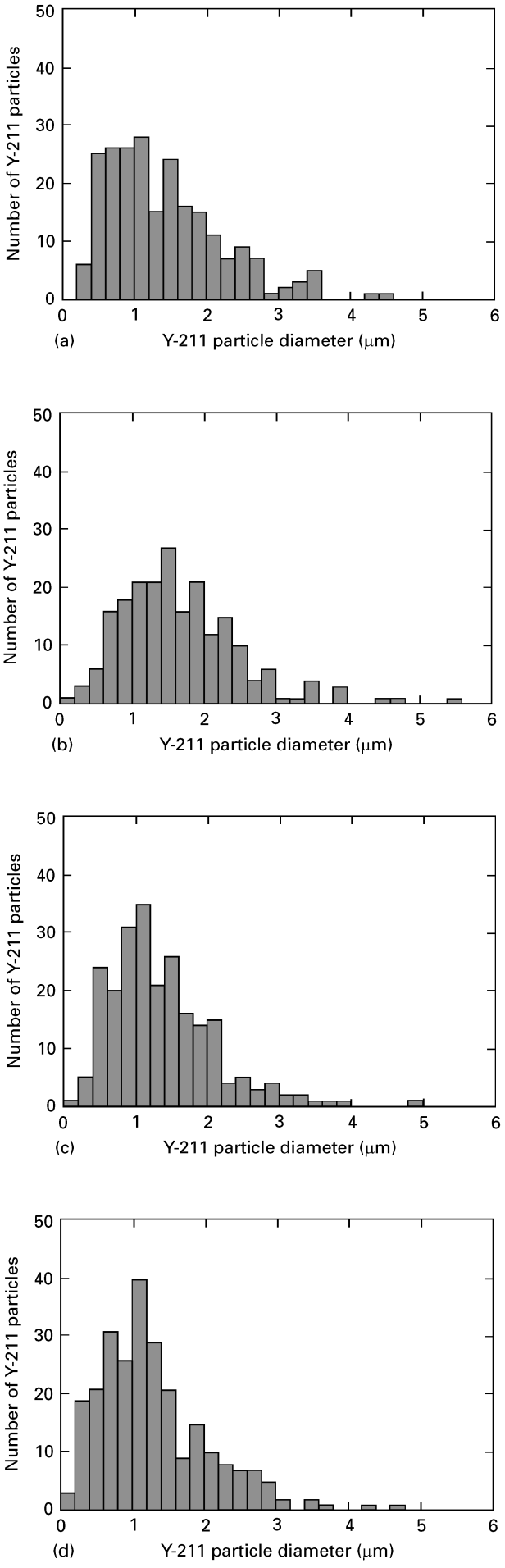

Figure 4 Distribution of the size Y-211 particles at a distance of (a) 85 μm, (b) 800 μm, (c) 2100 μm and (d) 3100 μm from the centre of the seed along the *a*/*b* direction of the grain.

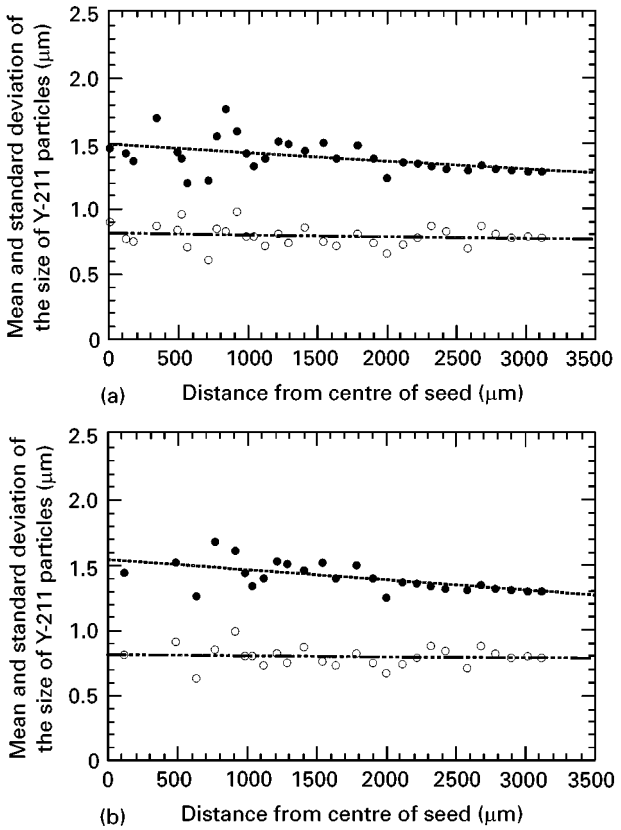

Figure 5 (●) Mean and (○) standard deviation of the size distribution of Y-211 particles as a function of the distance from the centre of the seed along the *a*/*b* direction of the grain with (a) lower and (b) higher sampling accuracy.

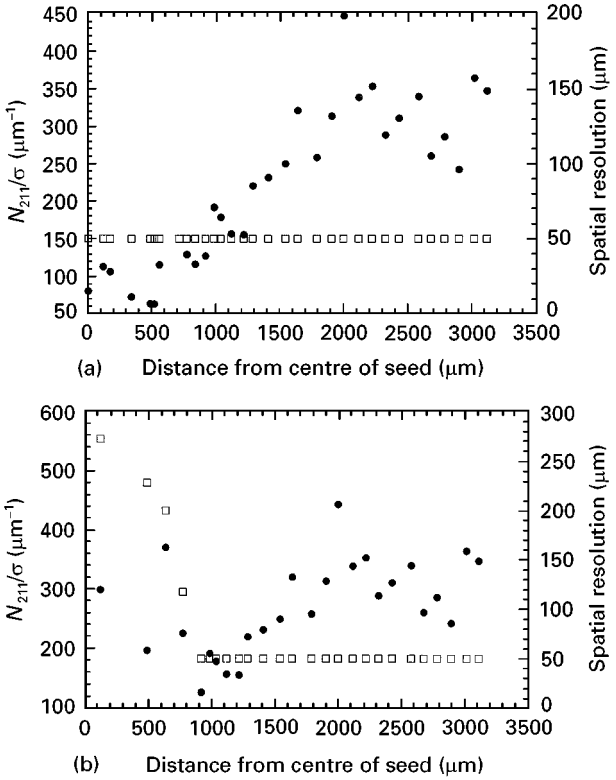

Figure 6 (●) Sampling accuracy (number of Y-211 particles/σ), and (□) spatial sampling resolution as a function of distance from the centre of the seed along the *a*/*b* axis of the grain for data with (a) lower and (b) higher sampling accuracy.

statistical accuracy of the results. This limitation can be overcome, however, by extending the area of analysis to include a larger number of Y-211 particles. Fig 5b was constructed by sampling a larger area in the vicinity of the seed and illustrates the gain in statistical accuracy that may be achieved by this technique.

The ratio of the number of Y-211 inclusions in a given sample area to the standard deviation of their size distribution (i.e. $n_{211}:\sigma$) is indicative of the statistical significance of the data. Fig. 6a shows the variation of this measure of sampling accuracy with distance from the centre of the seed and was derived from the data presented in Fig. 5a. The observed increase in $n_{211}:\sigma$ is due to the increase in number of Y-211 particles and a relatively constant value of σ (Figs 3b and 5b, respectively). In addition to sampling accuracy, the sampling area of the Y-211 particle density within the scanning electron micrographs provides a measure of the linear spatial resolution of the analysis, which was constant at 50 μm along the *a*/*b* axis of the grain, as shown in Fig. 6a. The low sampling accuracy of the data in the vicinity of the seed (also shown in this figure) is due primarily to the relatively low Y-211 number density and can be improved by increasing the sampling frequency by combining two or more micrographs, as shown in Fig. 6b. It can be seen from this figure that the sampling accuracy is improved significantly up to displacements of $\sim$900 μm from the seed at the expense of a reduced linear resolution of the analysis.

The above observations of the average size, number density and area fraction of Y-211 particles may be interpreted relative to particle pushing, ripening and coalescence effects which have been reported to take place during the melt-growth process. In general, larger Y-211 particles in the peritectic state have a higher surface energy than smaller particles and are therefore more susceptible to capture by the growing Y-123 phase (this occurs generally when the surface energy of the Y-211 particle in the peritectic state exceeds the sum of its surface energy when entrapped in the Y-123 phase and the surface energy of the solid–liquid interface [45]). On this basis an increase in the number density, and hence area fraction, of Y-211 particles may be anticipated with increasing distance from the seed as the more stable smaller particles are pushed along by the growth front, which is consistent with the results presented in Fig. 3a and b. The effect of the accumulation of smaller Y-211 particles during this process would be to reduce the average particle size with distance, which again is observed in the present study (Fig. 5). Hence our results are generally consistent with particle pushing theory during the YBCO peritectic solidification process. It should be noted, however, that the inevitable loss of liquid from the melt at elevated temperature could also account, at least in part, for the observed increase in Y-211 particle number density and area fraction with distance from the seed. It is likely, therefore, that a single mechanism is not responsible for observed features in the distribution of Y-211.

Y-211 particle ripening is the thermally activated growth of Y-211 particles in the peritectic state prior

to solidification. The solubility of yttrium in the BaCuO-rich liquid above the peritectic temperature, however, is low ($\sim$6%) [46] which suggests that any particle ripening would have to be supported by the slow erosion of other Y-211 particles in the liquid. As a result, the Y-211 particle number density may be expected to decrease slightly with distance from the seed as these "feeder" particles dissolve completely at elevated temperature. Further consequences of ripening would be to reduce the area fraction (the projected cross-sectional area of a single, large spherical particle of volume, V, is approximately 60% of that of the combined cross-sectional areas of two smaller particles of similar diameters, each of volume $V/2$) and to increase the average particle size with distance. These effects, which are exactly the opposite of the results observed in Figs 3a, b and 5, will be off-set to some degree by the loss of liquid from the sample at elevated temperature during melt processing, although this is not considered sufficiently large to account entirely for the observed trends.

The coalescence of Y-211 particles during melt growth would result clearly in a net decrease in number density with distance from the seed if the coalesced particles were counted singly, and to a decrease in area fraction (the argument applied to ripening applies equally to particle coalescence). Finally, this should be accompanied by an increase in the average particle size with distance. These effects are not observed experimentally, although liquid loss would reduce their magnitude, which again suggests that Y-211 particle coalescence is not a dominant mechanism in the development of Y-211 particles during the melt process.

On the basis of these results, particle pushing would appear to provide the most plausible explanation of the observed distribution of the Y-211 phase in seeded melt-processed samples. This mechanism, however, has a number of limitations which should be taken into account. Most importantly, particle pushing assumes that the Y-211 particles do not dissolve during the pushing process, which is clearly not the case in the YBCO system, because these particles represent the only source of yttrium. Y-211 particles must necessarily dissolve at the growth interface in order to propagate the Y-123 phase. Secondly, the Y-211 particles are of acicular, rather than spherical geometry, which tends to result in the alignment of their long axis either parallel or perpendicular to the growth direction [47]. This suggests that the growth front and Y-211 particles interact strongly at the growth interface which may reduce the effect of particle pushing. Finally, the addition of second phases such as platinum have been reported widely to reduce the average Y-211 particle size and to increase the number density, accordingly. The effects of such additions are to reduce the surface energy of the Y-211 particles (and hence liquid loss) which should also influence particle pushing. A similar study to that reported here on samples doped with platinum, however, shows that number density, area fraction and average particle size vary with distance from the seed in a similar manner to that shown in Figs 3a, b and 5 [48]. This suggests that the trends observed are less sensitive to surface-energy and liquid-loss considerations and that influences other than particle pushing may contribute to the properties of Y-211 inclusions in melt-processed YBCO.

In summary, a number of mechanisms are probably responsible for the observed variation in Y-211 number density, area fraction and average particle size with distance from the seed. Of these, particle pushing plays a significant role, although it is unlikely that this is the dominant mechanism. Particle ripening and coalescence and liquid loss all contribute to varying degrees, although it is not possible to quantify the extent of these contributions from the present study. These effects will be the subject of future publications.

4. Conclusion

Critical current density is closely related to the distribution of Y-211 particles in large-grain melt-processed YBCO. This characteristic, therefore, is particularly important for a range of high-field and high-current applications of this material. High-resolution secondary electron SEM image analysis has proved to be a powerful tool for investigating the key features of the Y-211 particle distribution, such as area fraction, number density and size. SEM image analysis of a large-grain YBCO sample (dimensions $8 \times 8 \times 3\ mm^3$), fabricated via seeded peritectic solidification, reveals that both the area fraction and the number density of the Y-211 particles increase continuously with distance from the centre of the seed towards the grain boundary (i.e. along the a/b directions of grain growth). The mean and standard deviation of the size distribution of the particles, on the other hand, were observed to decrease slightly with distance from the seed which suggests that the increase in area fraction can be attributed to an increase in number density of the Y-211 particle distribution across the specimen. Factors which may influence the measured area fraction, number density and average size of the Y-211 particles include particle pushing, grain coalescence, ripening effects and liquid loss. Of these, particle pushing appears to be the most dominant mechanism, although this is generally inconclusive. Further investigation of these factors will be the subject of a future study.

Acknowledgements

The authors gratefully acknowledge the support of the Croucher Foundation and British Nuclear Fuels Ltd.

References

1. F. C. MOON and P. Z. CHANG, *Appl. Phys. Lett.* **56** (1990) 22.
2. W. K. CHU, K. B. MA, C. K. McMICHAEL and M. A. LAMB, *Appl. Supercond.* **1** (1993) 1259.
3. M. MURAKAMI, *ibid.* **1** (1993) 1157.
4. H. FUKUYAMA, K. SEKI, T. TAKIZAWA, S. ENDOU, M. MURAKAMI, H. TAKAICHI and N. KOSHIZUKA, *Adv. Supercond.* **5** (1993) 1313.
5. R. TAKAHATA, H. YEYAMA and A. KUBO, *ibid.* **5** (1993) 1309.

6. C. P. BEAN, *Rev. Mod. Phys.* **36** (1964) 31.
7. D. F. LEE, V. SELVAMANIKAM and K. SALAMA, *Physica C* **165** (1990) 480.
8. M. MURAKAMI, S. KOTOH, N. KOSHIZUKA, S. TANAKA, T. MATSUSHITA, S. KAMBE and K. KITAZAWA, *Cryogenics* **30** (1990) 390.
9. S. SENGUPTA, D. SHI, Z. WANG, C. BIONDO, U. BALACHANDRAN and K. C. GORETTA, *Physica C* **199** (1992) 43.
10. V. CHAKRAPANI, D. BALKIN and P. McGINN, *Appl. Supercond.* **1** (1973) 71.
11. M. LEPROPRE, I. MONT, M. P. DELAMARE, M. HERVIEU, CH. SIMON, J. PROVOST, G. DESGARDIN, B. RAVEAU, J. M. BARBUT, D. BOURGAULT and D. BRAITHWAITE, *Cryogenics* **34** (1994) 63.
12. D. N. MATTHESS, J. W. COCHRANE and G. J. RUSSELL, *Physica C* **249** (1995) 255.
13. WAI LO, D. A. CARDWELL, C. D. DEWHURST and S. L. DUNG, *J. Mater. Res.* **11** (1996) 786.
14. T. S. LUHMAN, M. STRASIK, A. C. DAY, D. F. GARRIGUS, T. D. MARTIN, K. E. M'CRARY and H. G. AHLSTROM, *Appl. Supercond.* **148** (1995) 35.
15. S. JIN, R. SHERWOOD, E. M. GYORGY, T. H. TIEFEL, R. B. VAN DOVER, G. W. KAMMLOTT, R. A. FASTNACHT and H. D. KEITH, *Appl. Phys. Lett.* **52** (1988) 2074.
16. K. SALAMA, V. SELVAMANIKAM, L. GAO and K. SUN, *ibid.* **54** (1989) 2352.
17. M. MURAKAMI, *Mod. Phys. Lett. B* **4** (1990) 163.
18. M. MURAKAMI, S. GOTOH, H. FUJIMOTO, K. YAMAGUCHI, N. KOSHIZHKA and S. TANAKA, *Supercond. Sci. Technol.* **4** (1991) S49.
19. C. VARANASI and P. J. McGINN, *Mater. Lett.* **17** (1993) 205.
20. A. ENDO, H. S. CHAUHAN, T. EGI and Y. SHIOHARA, *J. Mater. Res.* **4** (1996) 795.
21. C. J. KIM, K. B. KIM and G. W. HONG, *Mater. Lett.* **21** (1994) 9.
22. P. K. ROHATGI, R. ASTHANA and F. YARANDI, in "Solidification of Metal Matrix Composites", edited by P. K. Rohatgi (TMS, Warrendale, PA, 1990) p. 51.
23. D. M. STEFANESCU and B. K. DHINDAW, in "Metals Handbook" Vol. 15 (ASM International, Metals Park, OH, 1988) p. 142.
24. I. M. LIFSHITZ and V. V. SLYOZOV, *J. Phys. Chem. Solids* **35** (1961) 35.
25. T. IZUMI, Y. NAKAMURA and Y. SHIOHARA, *J. Mater. Res.* **6** (1993) 1240.
26. C. VARANASI, P. J. McGINN, V. PAVATE and E. P. KVAM, *Physica C* **211** (1994) 46.
27. C. VARANASI, M. A. BLACK and P. J. McGINN, *J. Mater. Res.* **3** (1996) 565.
28. C. J. KIM, K. B. KIM and G. W. HONG, *Physica C* **232** (1994) 163.
29. L. DURAND, D. DIERICKX, P. REGNIER, O. VAN DER BIEST and S. POISSONNET, *Supercond. Sci. Technol.* **9** (1996) 290.
30. C. VARANASI and P. J. McGINN, *Physica C* **207** (1993) 79.
31. U. BALACHANDRAN, W. ZHONG, C. A. YOUNGDAHL and R. POEPPEL, *J. Electron. Mater.* **22** (1993) 1285.
32. C. J. KIM, K. B. KIM, D. Y. WON and G. W. HONG, *Mater. Lett.* **20** (1994) 283.
33. J. C. L. CHOW, WAI LO, H. T. LEUNG and D. A. CARDWELL, *J. Mater. Sci. Lett.* **15** (1996) 1833.
34. B. NI, M. KOBAYASHI, K. FUNAK, K. YAMAFUJI and T. MATSUSHITA, *Jpn J. Appl. Phys.* **32** (1993) L1861.
35. T. OKA, Y. ITOH, Y. YANAGI, H. TANAKA, S. TAKASHIMA, Y. YAMADA and U. MIZUTANI, *Physica C* **200** (1992) 55.
36. WAI LO, D. A. CARDWELL, S.-L. DUNG and R. G. BARTER, *J. Mater. Res.* **1** (1996) 39.
37. *Idem, J. Mater. Sci.* **30** (1995) 3995.
38. WAI LO, D. A. CARDWELL, C. D. DEWHURST and S.-L. DUNG, *J. Mater. Res.* **4** (1996) 786.
39. D. A. CARDWELL, WAI LO, H. D. E. THORPE and A. ROBERTS, *J. Mater. Sci. Lett.* **14** (1995) 1444.
40. D. A. CARDWELL, A. R. JONES, N. J. C. INGLE, A. M. CAMPBELL, T. W. BUTTON, N. McN. ALFORD, F. WELLHOFER and J. S. ABELL, *Cryogenics* **34** (1994) 671.
41. J. J. I. GOLDSTEIN, D. E. NEWBURY, P. ECHLIN, D. C. JOY, F. FIORI and E. LIFSHIN, "Scanning Electron Microscopy and X-ray Microanalysis" (Plenum Press, New York, 1981) pp. 176–8.
42. I. M. WATT, "The Principles and Practice of Electron Microscopy" (Cambridge University Press, Cambridge, UK (1985) pp. 47–50.
43. S. K. KURTZ and F. M. A. CARPAY, *J. Appl. Phys.* **51** (1980) 5725.
44. H. T. LEUNG, W. LO, J. C. L. CHOW and D. A. CARDWELL, in preparation.
45. W. LO, H.-T. LEUNG, D. A. CARDWELL and J. C. L. CHOW, *J. Am. Ceram. Soc.* **80** (1997) 813.
46. M. J. CIMA, M. C. FLEMINGS, A. M. FIGUEREDO, M. NAKADE, H. ISHII, H. D. BRODY and J. S. HAGGERTY, *J. Appl. Phys.* **76** (1992) 179.
47. D. A. CARDWELL, W. LO, H.-T. LEUNG and J. C. L. CHOW, *Adv. in Supercond.* **IX 2** (1997) 725.
48. J. C. L. CHOW, W. LO, C. D. DEWHURST, H.-T. LEUNG, D. A. CARDWELL and Y. H. SHI, *Supercond. Sci. Technol.* **10** (1997) 435.

Received 11 July 1996
and accepted 22 August 1997